WATER RESOURCES RESEARCH, VOL. 31, NO. 4, PAGES 913–924, APRIL 1995

Solving the estimation-identification problem in two-phase flow modeling

Stefan Finsterle and Karsten Pruess
Earth Sciences Division, Lawrence Berkeley Laboratory, University of California, Berkeley

Abstract. In this paper a procedure is presented to solve the estimation-identification problem in two-phase flow modeling. Given discrete observations made on the system response, an optimum parameter set is derived for an appropriate conceptual model by solving the inverse problem using standard optimization techniques. Subsequently, a detailed error analysis is performed, and nonlinearity effects are considered. We discuss the iterative process of model identification and parameter estimation for a ventilation test performed at the Grimsel Rock Laboratory, Switzerland. A numerical model of the ventilation drift and the surrounding crystalline rock matrix is developed. Evaporation of moisture at the drift surface and the propagation of the unsaturated zone into the formation are simulated. A sensitivity analysis is performed to identify the parameters to be estimated. Absolute permeability and two parameters of van Genuchten's characteristic curves are subsequently determined based on measurements of negative water potentials, evaporation rates, and gas pressure data. The performance of the minimization algorithm and the system behavior for the optimum parameter set are discussed. The study shows that a field experiment conducted under two-phase flow conditions can be successfully reproduced by taking into account a variety of physical processes and that it is possible to reliably determine the two-phase hydraulic properties that are related to the given conceptual model.

1. Introduction

Mathematical-numerical models commonly used to analyze or predict the response of groundwater systems have increasing capabilities for dealing with complex flow and transport processes. Simulation tools for nonisothermal flow of multiphase, multicomponent fluids have been developed for various applications to geothermal reservoir engineering, nuclear waste isolation studies, and unsaturated zone hydrology. However, greater model sophistication is usually accompanied by an increasing number of hydrogeologic parameters which enter the governing equations to describe the interaction between the fluids and the porous media. While some of the parameters affecting fluid flow in partially saturated formations can be obtained directly from laboratory experiments, such measured parameters may differ significantly from their model counterparts both conceptually and numerically, mainly because of scale effects. In order to obtain model-related formation parameters, the strategy is to calibrate the numerical model using observations of the system response at discrete points in space and time. The methodology of parameter estimation for saturated flow was reviewed by *Carrera and Neuman* [1986] and *Yeh* [1986]. Similar techniques have been applied to estimate parameters for unsaturated flow and transport processes (for a review see *Kool et al.* [1987]).

Three main aspects have to be considered when dealing with inverse modeling. The first and most important is referred to as model conceptualization. Model conceptualization can be defined as the process of approximating the relevant factors that control the behavior of the real flow system. It includes the specification of the flow system geometry, formulation of constitutive relationships for multiphase flow, parametrization of the model domain, and the definition of appropriate initial and boundary conditions. While conceptualization is part of any modeling effort, it is important to realize that the parameters estimated by means of calibration procedures are only meaningful within the framework of the given conceptual model. Strictly speaking, they are model parameters rather than aquifer parameters. The second input to inverse modeling is the data. The type of quantities to be measured, the locations of the observation points, and the duration of each measurement period have to be selected so that the parameters to be estimated are sensitive with respect to the data. Furthermore, most optimization procedures require some prior estimates of the measurement errors. The third aspect deals with the actual procedure of how to derive model parameters from the data observed in the field.

Modeling is an iterative process of developing model structures, for which an optimum parameter set is sought, followed by an interpretation of the remaining residuals which may point toward aspects of the model that need to be modified. Residual analysis for model identification requires a good deal of expertise and a sound understanding of the system behavior under two-phase flow conditions. Note, however, that the step of quantifying the parameters for a given model structure can be carried out based on rather objective mathematical criteria. On the other hand, model conceptualization involves more qualitative information and may be guided by the overall purpose of the modeling effort.

The most widely employed approaches to solve the inverse problem minimize some norm of the differences between observed and model-predicted state variables. If taking the view of maximum likelihood, the performance criterion reflects the

Paper number 94WR03038.
0043-1397/95/94WR-03038$05.00

probability density function of the final residuals. For normally distributed residuals correlated in space and time, it can be shown that maximizing the probability of reproducing the observed data leads to a method known as generalized nonlinear least squares estimation, for which a variety of optimization procedures have been developed (see, for example, *Scales* [1985]). If the model is nonlinear in the parameters, minimization of the objective function is an iterative process in which information about the gradient and the convexity of the objective function is used to perform a downhill step toward a local or global minimum. One of the most generally applicable algorithms is the one proposed by *Levenberg* [1944], which was improved by *Marquardt* [1963]. The basic idea of the Levenberg-Marquardt method is to move along the steepest descent direction far from the minimum and to switch continuously to the Gauss-Newton algorithm as the minimum is approached.

The strong nonlinearities inherent in two-phase flow make it difficult to minimize the objective function in an efficient and stable way. Reparametrization, such as logarithmic transformation of absolute permeabilities, and the incorporation of prior information about the parameters have been proposed to improve the properties of the objective function. Additionally, the robustness of the solution has to be questioned because the residuals almost never obey a Gaussian distribution. The assumption of normally distributed residuals is convenient because it leads to very powerful optimization procedures but may not be justified, mainly because of two reasons. First, the errors associated with field data typically show many more outlier points than one would expect from the tail of the normal distribution. Second, a simulation model is only able to reproduce an average trend of the true system behavior because of the incompleteness and inaccuracy of the underlying conceptual model. As a result, the residuals, which contain both model and measurement errors, may have a substantial contribution from deviations which are systematic rather than random; consequently, they cannot be properly described by statistical measures. Nevertheless, least squares optimization has proved successful in many applications. Only a few alternative approaches have been proposed in the field of groundwater hydrology (for an example see *Xiang et al.* [1993]).

The numerical model used to simulate nonisothermal two-phase flow is described in the next section. Subsequently, the formulation of an objective function and its minimization are presented. The linearity assumption of the standard error analysis will be discussed in detail. Finally, the proposed method is applied to field data from an experiment performed at the Grimsel Rock Laboratory, Switzerland. Two-phase flow parameters for a crystalline rock matrix are estimated based on measurements of negative water potential, gas pressure, and water inflow to a ventilated drift section.

2. The Direct Problem

Given a conceptual model of the physical system and a set of values of the model parameters, the prediction of the system response for arbitrary initial and boundary conditions is referred to as the direct problem. In this work the direct problem is solved by using the two-phase two-component numerical simulator TOUGH2 [*Pruess*, 1987, 1991]. Consider a system with two mobile phases $\beta(\beta = g$: gas; $\beta = l$: liquid), and two components κ ($\kappa = a$: air; $\kappa = w$: water). The governing mass balance equation for each component can be written in the following integral form [*Pruess and Narasimhan*, 1985]:

$$\frac{\partial}{\partial t}\int_V M^\kappa\, dv = \int_\Gamma \mathbf{F}^\kappa \cdot \mathbf{n}\, d\Gamma + \int_V q^\kappa\, dv \tag{1}$$

The integration is over an arbitrary subdomain V of the flow system, which is bounded by the closed surface Γ, with inward normal vector $\mathbf{n}$. M^κ is the mass accumulation term for component κ, $\mathbf{F}^\kappa$ is the mass flux term, and q^κ is a term representing sinks and sources. The mass accumulation term is

$$M^\kappa = \phi \sum_{\beta=l,g} S_\beta \rho_\beta X_\beta^\kappa \tag{2}$$

where ϕ is porosity, S_β is phase saturation, ρ_β is density of phase β, and X_β^κ is the mass fraction of component κ in phase β. Thus M^κ is the total mass of component κ present per unit volume.

The mass flux terms contain a sum over the two phases

$$\mathbf{F}^\kappa = \sum_{\beta=l,g} \mathbf{F}_\beta X_\beta^\kappa \tag{3}$$

where the flux of phase β is

$$\mathbf{F}_\beta = -k\frac{k_{r\beta}}{\mu_\beta}\rho_\beta(\nabla P_\beta - \rho_\beta \mathbf{g}) - \delta_{\beta g} D_{wa}\rho_\beta \nabla X_\beta^\kappa \tag{4}$$

Here, k denotes absolute permeability, $k_{r\beta}$ is relative permeability of phase β as a function of saturation, μ_β is dynamic viscosity of phase β, P_β is the pressure in phase β, and $\mathbf{g}$ is gravitational acceleration. The last term in (4) contributes only to gas phase flow and represents the diffusive flux, with D_{va} the diffusion coefficient for vapor-air mixtures in porous media [*Vargaftik*, 1975; *Walker et al.*, 1981]

$$D_{va} = \Omega^\kappa D_{va}^0 \frac{P_0}{P_g}\left(\frac{T}{T_0}\right)^\theta \tag{5}$$

where D_{va}^0 is the vapor diffusivity at standard conditions T_0 and P_0 and θ is a material parameter to account for temperature dependency. The parameter Ω^κ specifies properties relevant to binary diffusion in a porous medium. For air, it describes the restriction of the molecular diffusion to the gas-filled fraction of the pore space, $\Omega^a = \tau\phi S_g$, where τ is a tortuosity factor. However, there is a great deal of evidence from studies in soil sciences that diffusion of vapor is enhanced by pore-level phase change processes [*Walker et al.*, 1981]. The experimentally determined values Ω^w for vapor diffusion may be much larger than the parameter group $\tau\phi S_g$ for air diffusion.

Binary diffusion becomes an important factor for moisture transfer if large temperature gradients or strong capillary forces are present. The latter induce a decrease in the vapor partial pressure P_v according to Kelvin's equation [*Edlefsen and Anderson*, 1943]:

$$P_v = P_{\text{sat}} \exp\left[P_c M_w/\rho_l RT\right] \tag{6}$$

where P_{sat} is saturated vapor pressure for a given absolute temperature T, $P_c = P_l - P_g$ is the capillary pressure, R is the universal gas constant, and M_w is the molecular weight of water. As a result, a capillary pressure gradient leads to a mass fraction gradient ∇X_g^κ, which is the driving force for binary diffusion.

As part of the model conceptualization, a parametric relationship has to be chosen to describe the two-phase hydraulic

properties. *Luckner et al.* [1989] derived a consistent set of capillary pressure and relative permeability curves based on van Genuchten's model [*van Genuchten*, 1980]. The macroscopic capillary pressure P_c can be related to saturation as follows:

$$P_c = -\frac{1}{\alpha}(S_e^{-1/m} - 1)^{1/n} \tag{7}$$

with the effective liquid saturation

$$S_e = \frac{S_l - S_{lr}}{1 - S_{lr}} \qquad S_{lr} < S_l < 1 \tag{8}$$

where S_{lr} is the residual liquid saturation. The parameter α can be interpreted as the reciprocal of the air entry pressure, and parameter n reflects the pore size distribution of the porous medium. With $m = 1 - 1/n$, and applying Mualem's predictive hydraulic conductivity model [*Mualem*, 1976], expressions for liquid and gas relative permeabilities are derived [*Luckner et al.*, 1989], yielding

$$k_{rl} = S_e^{\eta}[1 - (1 - S_e^{1/m})^m]^2 \tag{9a}$$

$$k_{rg} = (1 - S_e)^{\gamma}[1 - S_e^{1/m}]^{2m} \tag{9b}$$

where η and γ are pore connectivity parameters for the wetting and nonwetting phases, respectively.

The thermophysical properties of liquid water and vapor are obtained from steam table equations [*International Formulation Committee*, 1967]. Air is treated as an ideal gas, and gas phase pressure is assumed to be the sum of air and vapor partial pressures. Air dissolution in liquid water is represented by Henry's law.

In order to describe the thermodynamic state of a three-component (water, air, and heat) system in which local equilibrium is assumed, it is necessary to choose three primary state variables and a set of secondary variables which include thermodynamic and transport properties such as densities, relative permeabilities, viscosities, mass fractions, enthalpies, etc. The three variables must be chosen so that they are independent of each other and that the entire set of secondary variables can be derived. In multiphase flow problems involving phase transitions, a different set of variables has to be used for each potential phase combination. We have chosen pressure, temperature, and air mass fraction as the primary thermodynamic variables for single-phase (either gas or liquid) and pressure, gas saturation, and temperature for two-phase conditions. Other choices of primary variable sets are discussed in *Peaceman* [1977]. The governing transport equations are discretized in space by using an integral finite difference formulation [*Narasimhan and Witherspoon*, 1976]. Time is discretized fully implicitly as a first-order finite difference. Discretization results in a set of nonlinear coupled algebraic equations which are solved by means of Newton-Raphson iterations. A generalized minimum residual conjugate gradient algorithm is used to solve the linear equations arising at each iteration step [*Seager*, 1988].

3. The Inverse Problem

3.1. Objective Function

The determination of hydraulic parameters based on a set of observed state variables is referred to as the inverse problem. Any input parameter of the numerical model can be subjected to the estimation process. These are, for example, the absolute permeability or the parameters of the characteristic curves. Furthermore, initial and boundary conditions as well as geometrical features such as fracture spacing can be considered unknown parameters. The parameters may refer to individual points, to elements of the discretized flow region, or to zones for which their values are assumed to be constant. The objective of the inverse model is to provide improved estimates of these parameters by relying on certain measurements. Potential observation types are those which correspond to or can be derived from the model output, for example, gas pressure, water potential, liquid flow rate, temperature, and saturation measurements. Prior information about any of the parameters mentioned above can be added to the vector of observable variables. The indirect approach to inverse modeling consists of minimizing a performance criterion that measures the differences between observed and computed system response. The residual vector $\mathbf{r}$ assembles vectors $\mathbf{r}_j$, which contain contributions from data of a certain type j, $j \in$ {prior information, pressure, flow rate, saturation, $\cdots$}

$$\mathbf{r}_j = \mathbf{y}_j^* - \mathbf{y}_j(\mathbf{p}) \tag{10}$$

where $\mathbf{y}_j^*$ is the vector of the observed state variables of type j and $\mathbf{y}_j$ contains the corresponding model output which is a function of the unknown parameter vector $\mathbf{p}$. The number of elements in $\mathbf{r}_j$ is equal to the number of points in space and time for which data are available. The error structure of the residuals is assumed to be Gaussian and can therefore be described by a covariance matrix as follows:

$$\mathbf{C}_j = (\sigma_0^2)_j \mathbf{V}_j \tag{11}$$

The scalar σ_0^2 can be termed the prior error variance. It is introduced to control the relative importance of observations of different types. For prior information, σ_0^2 can be interpreted as a weighting coefficient for the physical plausibility criterion [*Neuman*, 1973], or it can be used as a regularization parameter to improve the well-posedness of the nonlinear least squares problem [*Chavent*, 1991]. With $\mathbf{V}_j$ being a positive definite matrix representing the relative error structure of observations at different points in space and time, $\mathbf{C}_j$ reflects the expected uncertainty of the residuals of type j. If the quality of the data is not well known, one might consider estimating the statistical parameters along with the other model parameters, for example, by using the iterative procedure proposed by *Carrera and Neuman* [1986]. Provided that observations of different types are uncorrelated, the objective function to be minimized reads

$$\zeta(\mathbf{p}) = \sum_j [\sigma_0^{-2}\mathbf{r}^T\mathbf{V}^{-1}\mathbf{r}]_j \tag{12}$$

Equation (12) is the sum of the squared residuals weighted by the inverse of the prior covariance matrix. This formulation is identical to the general concepts used for solving coupled inverse problems as described by *Sun and Yeh* [1990]. The estimator corresponding to (12) is known as the generalized nonlinear least squares estimator. Based on maximum likelihood theory, it can be shown that minimizing ζ is equivalent to maximizing the probability of reproducing the observed system state, provided that the residuals follow a Gaussian distribution. Note that because of the normality assumption inherent in least squares formulations, the estimator leads to biased results if large residuals occur more frequently than predicted

by the normal distribution. In these cases, the objective function should be appropriately modified to improve the robustness of the estimator (for details see *Finsterle* [1993b]).

3.2. Minimization Algorithm

An appropriate algorithm is needed to minimize the objective function ζ. The least squares formulation suggests use of Newton-type minimization algorithms with quadratic convergence near the optimum. In Newton's method, the objective function is locally approximated by a quadratic form which allows iterative computation of an improved parameter vector $\mathbf{p}_{new}$ from a previous estimate $\mathbf{p}_{old}$ as follows:

$$\mathbf{p}_{new} = \mathbf{p}_{old} - \mathbf{H}^{-1}(\mathbf{p}_{old}) \cdot \mathbf{g}(\mathbf{p}_{old}) \tag{13}$$

where $\mathbf{g}$ is a gradient vector and $\mathbf{H}$ is the Hessian matrix. We mention in passing that (13) is a closed-form solution for the unknown parameters if the model is linear. The Hessian matrix $\mathbf{H}$ is not only expensive to calculate but may also become negative-definite if the model is strongly nonlinear. Levenberg has proposed a method to approximate the Hessian by a matrix $\mathbf{H}'$ that is easy to calculate and always positive definite [*Levenberg*, 1944]:

$$\mathbf{H}' = \mathbf{J}^T\mathbf{C}^{-1}\mathbf{J} + \mu\mathbf{D} \tag{14}$$

Here, $\mathbf{C}$ is the assembled covariance matrix which includes all observation types. It has a block diagonal structure with submatrices $\mathbf{C}_j$. Accordingly, $\mathbf{J}$ is the assembled Jacobian matrix of dimension $m \times n$ with elements $J_{ik} = \partial r_i/\partial p_k$, where m is the total number of observations, n is the number of parameters to be estimated, and r_i is the ith element of the assembled residual vector $\mathbf{r} = (\mathbf{r}_{pi}, \mathbf{r}_{pres}, \mathbf{r}_{flow}, \ldots, \mathbf{r}_{sat})^T$, containing all residual vectors $\mathbf{r}_j$ for which data are available. $\mathbf{D}$ denotes a diagonal matrix of order n with elements equivalent to the diagonal elements of matrix $(\mathbf{J}^T\mathbf{C}^{-1}\mathbf{J})$. The scalar $\mu \geq 0$ is the so-called Levenberg parameter. A large value of μ represents a small step in the steepest descent direction, whereas for $\mu \to 0$, (13) converges to a Gauss-Newton step. *Marquardt* [1963] has given a simple rule of how to continuously update the Levenberg parameter μ during the optimization procedure, switching from a gradient step far from the minimum to a Gauss-Newton step if the minimum is approached. The reason for choosing the Levenberg-Marquardt algorithm is its robustness far from the optimum, where the topology of the objective function may be complicated because of the nature of the two-phase flow formulation. Furthermore, when approaching the optimum, nonlinear effects are somewhat reduced, which allows use of Gauss-Newton steps near the minimum.

3.3. Error Analysis

An uncertainty measure of the estimated parameter values is usually obtained under the assumption of normality and linearity. The normality assumption is based on the fact that the distribution of a sum of random values always tends toward normal if the sample size is sufficiently large. The linearity assumption postulates that the model output can be approximated by a linear function of the parameters within the area covered by the confidence region. Both assumptions have to be questioned for parameter estimation in groundwater hydrology because the sample size is usually small and the two-phase flow model is highly nonlinear. In this section, we first derive the covariance matrix for the linear case. We then discuss a procedure originally proposed by *Carrera* [1984] to better approximate the true confidence region in the nonlinear case.

The $100(1 - \alpha)\%$ confidence region for the true but unknown parameter vector $\bar{\mathbf{p}}$ contains those values $\mathbf{p}$ for which [*Donaldson and Schnabel*, 1987]

$$\zeta(\mathbf{p}) - \zeta(\hat{\mathbf{p}}) \leq s_0^2 n F_{n,m-n,1-\alpha} \tag{15}$$

where $\hat{\mathbf{p}}$ is the vector holding the optimum parameter set, s_0^2 is the estimated residual variance, and $F_{n,m-n,1-\alpha}$ is a quantile of the F distribution. Here, α is the probability that the hypothesis is rejected even though it is true. In the general case, this confidence region is of arbitrary shape, bounded by the points of constant likelihood. Its construction requires solving the direct problem many times in order to produce the corresponding contour of the objective function. Linearization methods have the advantage that the resulting confidence region is ellipsoidal, making it inexpensive to construct and easy to report. For a maximum likelihood estimator, the variance-covariance matrix is asymptotically given by

$$\hat{\mathbf{C}} = s_0^2\mathbf{H}(\hat{\mathbf{p}})^{-1} \tag{16}$$

where a circumflex indicates that the quantity is an a posteriori estimate. By linearizing the model $\mathbf{y}(\mathbf{p})$ using the affine approximation around $\hat{\mathbf{p}}$,

$$\mathbf{y}(\mathbf{p}) \approx \mathbf{y}(\hat{\mathbf{p}}) + \mathbf{J}(\hat{\mathbf{p}}) \cdot (\mathbf{p} - \hat{\mathbf{p}}) \tag{17}$$

we obtain for the covariance matrix of the estimated parameter set the expression

$$\hat{\mathbf{C}} = s_0^2(\mathbf{J}^T\mathbf{V}^{-1}\mathbf{J})^{-1} \tag{18}$$

with

$$s_0^2 = \frac{\mathbf{r}^T\mathbf{V}^{-1}\mathbf{r}}{m - n} \tag{19}$$

Since the estimated error variance s_0^2 is a random variable, it can be tested against the prior error variance σ_0^2. If the deviation between the two values is statistically significant, then the conceptual model provides an unlikely match to the data. Consequently, the estimated parameter set has to be questioned as well. A failure of the model test may also indicate a too optimistic assumption about the prior error structure of the residuals.

We can construct the confidence region for the linearized case consisting of those values $\mathbf{p}$ for which

$$(\mathbf{p} - \hat{\mathbf{p}})^T\hat{\mathbf{C}}^{-1}(\mathbf{p} - \hat{\mathbf{p}}) \leq nF_{n,m-n,1-\alpha} \tag{20}$$

The confidence region given by (20) is a succinct representation of the region defined by (15). Recall that the covariance matrix $\hat{\mathbf{C}}$ approximates the actual surface of the objective function at its minimum by a tangent hyperellipsoid under the assumption of normality and linearity. If the model is nonlinear, the coverage of the confidence region by the linear approximation may be very poor with respect to both its size and its shape. Reparametrization is a possibility to reduce nonlinearity effects and the asymmetry of the confidence region.

Let us now assume that the shape of the confidence region is close to ellipsoidal and that the orientation of the hyperellipsoid in the n-dimensional parameter space is accurately obtained from the linear error analysis. Then, by only adjusting the size of the hyperellipsoid, we can better approximate the confidence region without losing the advantage of producing

easily understandable results which are also simple to report. *Carrera* [1984] proposed a correction for the covariance matrix to account for nonlinearity. We adapt his basic idea of comparing the actual likelihood function with the results from the linear approximation at discrete points in the parameter space. These test points are preferably located along the main axis of the hyperellipsoid, i.e.,

$$\tilde{\mathbf{p}}_{i\pm} = \hat{\mathbf{p}} \pm (nF_{n,m-n,1-\alpha})^{1/2} a_i \mathbf{u}_i \qquad i = 1, \cdots, n \tag{21}$$

Here, $\tilde{\mathbf{p}}_{i\pm}$ are two test parameter sets on the ith axis, the direction of which is given by the eigenvector $\mathbf{u}_i$ of the covariance matrix $\hat{\mathbf{C}}$. Note that the distance from the optimal parameter set $\hat{\mathbf{p}}$ is selected as a multiple of the corresponding eigenvalue a_i^2 and the quantile of the F distribution. This means that the correction is tailored to approximate the confidence region on a certain confidence level $1 - \alpha$. The eigenvalues a_i^2, which represent the length of the semiaxis, are now corrected as follows:

$$a'^2_i = a_i^2 s_0^2 \left(\frac{A_+ + A_-}{2} \right)_i \tag{22}$$

with

$$A_{\pm i} = \frac{nF_{n,m-n,1-\alpha}}{\zeta(\tilde{\mathbf{p}}_{i\pm}) - \zeta(\hat{\mathbf{p}})} \tag{23}$$

Finally, the new covariance matrix is back-calculated from the eigenvectors $\mathbf{u}_i$ and the updated eigenvalues a'^2_i. The proposed correction requires $2n$ additional solutions of the direct problem and is thus relatively inexpensive. While the resulting confidence region is ellipsoidal by definition, the differences between $\zeta(\tilde{\mathbf{p}}_+)$ and $\zeta(\tilde{\mathbf{p}}_-)$ provide, as a byproduct of the correction procedure, some insight into the asymmetry of the true confidence region.

4. Application to Field Data

4.1. Introduction and Problem Description

The inverse modeling formulation outlined in the previous section has been implemented in a computer program named ITOUGH2 [*Finsterle*, 1993b], which has been verified by applying the code to synthetic test cases [*Finsterle*, 1993a]. The purpose of this section is to illustrate the applicability of the proposed methodology to field data that reveal strong two-phase flow effects.

A series of ventilation tests have been conducted at the Grimsel Rock Laboratory, Switzerland, a research facility operated by Nagra, the Swiss National Cooperative for the Disposal of Radioactive Waste. Ventilation tests were originally conceived to determine the macropermeability of crystalline rocks by measuring the total inflow into drift sections with controlled ventilation. In these tests, ventilation is viewed simply as a convenient means to convey the incoming moisture to a measuring device [*Kull et al.*, 1991]. Accordingly, the standard interpretation of these tests is based on assuming that flow toward the drift is single-phase liquid. However, the estimated matrix permeabilities may be affected by partial drying of the drift wall, leading to regions that are dominated by two-phase flow effects. In order to quantify the extent of the two-phase region and study its hydraulic properties, a joint project between the Institute of Terrestrial Ecology, Eidgenössische Technische Hochschule Zurich, and Nagra has been initiated. In situ measurements of water potential, water content, temperature, and ambient air humidity were performed during a ventilation test starting November 26, 1991 [*Gimmi et al.*, 1992].

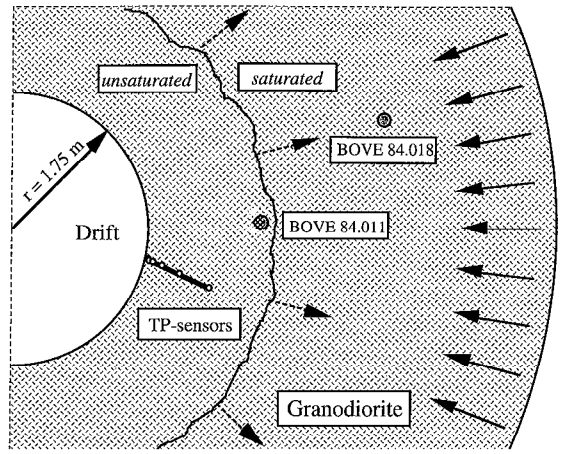

Figure 1. Schematic of model domain. TP, thermocouple psychrometer.

The ventilation experiment is conceptualized as follows (see Figure 1). We expect the flow regime to be radial in the vicinity of the drift. The computational region extends from the drift wall of radius 1.75 m to a presumably unaffected outer boundary at a distance of 6.75 m. A constant pressure of 0.37 MPa is prescribed at the outer boundary, reflecting the undisturbed pressure at drift level. The impact of gravity is neglected. The flow region is partitioned into 200 grid blocks with logarithmically increasing radial distances. The experimental site is located in mildly deformed granodiorite that is considered homogeneous on the scale of interest. Two boreholes (BOVE 84.011 and BOVE 84.018) were drilled parallel to the drift. They are equipped with conventional pressure transducers to observe the hydraulic head. Thermocouple psychrometers (TP) were installed at six different depths (2, 5, 10, 20, 40, and 80 cm from the drift wall). They measure negative water potentials in the partially saturated region as a function of time. An estimate of the total inflow to large, sealed-off sections of the drift is obtained from measurements of the moisture extracted from the circulated air in a cooling trap. On a much smaller scale, the evaporation rate at the drift surface is estimated by measuring gradients of relative humidity and temperature [*Vomvoris and Frieg*, 1991].

4.2. Simulation Results

In this section, we describe the formulation of the direct problem and the simulation results using the optimum parameter set. The determination of the parameter values will be discussed in section 4.3.

Prior to ventilation, the system is run to steady state in order to obtain the initial pressure and saturation distribution and to evaluate the inflow to the drift under almost fully liquid-saturated conditions. Notice that by reducing the pressure in the drift, air which is dissolved in the liquid phase comes out of solution, leading to a very small initial gas saturation throughout the model domain. When ventilation begins, formation water evaporates at the surface because of the reduced relative humidity, which is the main driving force for the desaturation of the formation. *Connell and Bell* [1993] show that the transfer

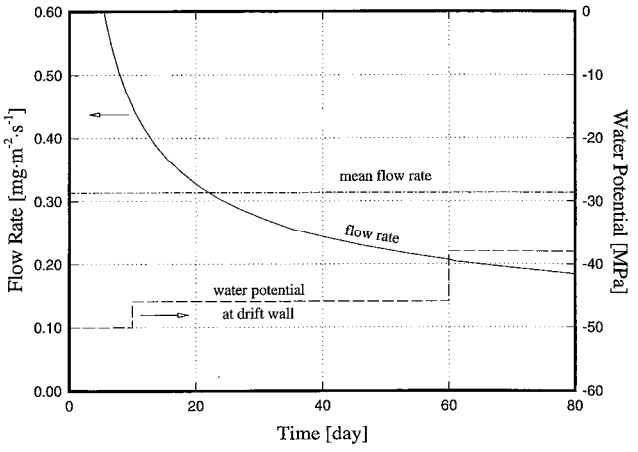

Figure 2. Flow rates and suction pressure at the drift wall as a function of time.

of moisture at a free surface is a complicated mechanism which depends on factors such as relative humidity, temperature gradient, wind velocity in the drift, and surface roughness, the latter two defining the thickness of the laminar boundary layer and the magnitude of the effective vapor diffusion coefficient at the drift wall. Rather than explicitly model the moisture transfer across the drift surface, the reduced relative humidity is imposed as a boundary condition at the drift wall, giving rise to an equivalent capillary suction according to Kelvin's equation [*Edlefsen and Anderson*, 1943]:

$$P_{c,\mathrm{equ}} = \ln(h)\rho_l \frac{RT}{M_w} \tag{24}$$

The relative humidity h in the drift is 68% at a temperature of 12.5°C during the first 10 days of the experiment, 71% at $T = 13.0$°C for the next 50 days, and 75% during the remaining 20 days, invoking an equivalent capillary suction of −50.0, −46.0, and −38.0 MPa, respectively. By prescribing these values directly at the drift wall, we neglect the variation in the vapor content in the boundary layer as a function of wind velocity and the actual evaporation rate. A sensitivity study was performed to assess the robustness of this model conceptualization. It turned out that the system behavior is relatively insensitive to the boundary suction pressure and the strength of the vapor diffusion at the drift wall. This is mainly because the evaporation rate is limited by the water supply from the formation, which is governed by the two-phase characteristics of the rock. Increased evaporation at the surface leads immediately to higher gas saturations at the drift wall, which reduces the liquid relative permeability, thus limiting the water supply for evaporation. The finding that the water inflow to the drift is relatively stable is also confirmed by the results of discrete evaporation measurements near the drift wall [*Vomvoris and Frieg*, 1991]. These data show that the temporal variations in evaporation rates due to changing climate conditions in the drift are very minor compared with the dramatic change in the equivalent suction pressure.

Figure 2 shows the calculated flow rate into the drift as a function of time. It can be seen that the flow rate does not seem to be affected by the changes in the relative humidity and associated capillary pressure at the drift wall. The average flow rate of water over 80 days in both liquid and vapor phases is 0.31 mg m^{-2} s^{-1}, which is larger than the steady state inflow under single-phase liquid conditions. Obviously, there is an increase in the amount of moisture that is removed from the formation by evaporation. However, since the flow regime is radial and finite, the system tends toward equilibrium between the evaporation rate at the drift surface and the incoming liquid from the formation, so that the expansion of the unsaturated zone slows down over time. The net loss of liquid in the model region is compensated for by a counterflow of gas from the drift into the formation.

Figure 3 depicts the pressure profile prior to ventilation and the final distribution after 80 days. The gas pressure throughout the partially saturated zone is close to atmospheric. The presence of the low pressure region shown in Figure 3 is consistent with the data obtained in the two boreholes BOVE 84.011 and BOVE 84.018, observations which led to speculations about the impact of the unsaturated zone on head and inflow measurements [*Vomvoris and Frieg*, 1991]. Here, "low pressures" are defined as pressures which are lower than those one might expect from a radial, single-phase flow field, i.e., the pressure profile prior to ventilation as shown in Figure 3, or the pressures observed in a nearby, almost saturated fracture zone [*Vomvoris and Frieg*, 1991]. At the end of the experiment, the computed gas pressure compares well with the values measured in the boreholes. Note that the formation is partially desaturated by evaporation to a radial distance of about 4 m. However, gas saturations greater than 50% are found only to a depth of a few centimeters from the drift surface. One should realize that the shape of the saturation profile depends strongly on the parametric model that describes the capillary pressure as a function of liquid saturation.

4.3. Inverse Modeling Results

Input parameters for the conceptual model described above are determined by inverse modeling. Three decisions have to be made. First, the calibration points in space and time must be selected. We choose 25 logarithmically spaced points in time during a ventilation period of 80 days and compare the calculated water potentials with the tensiometer measurements at six different depths. Second, we assume that the standard deviations of the residuals are 10% of the measured values and that they are uncorrelated. Third, we have to decide which parameters shall be subjected to the optimization process. The

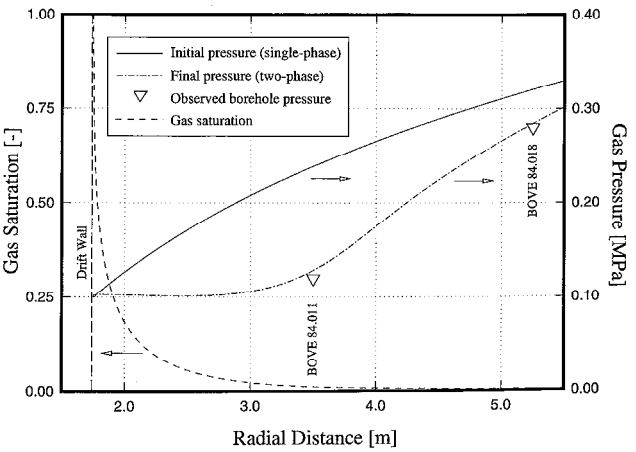

Figure 3. Gas saturation and pressure profiles. The measured borehole pressures are shown as triangles.

Table 1. Sensitivity Analysis for Identification of Model Parameters That Will Be Subjected to the Optimization Process

Parameter	Value	Sensitivity Coefficient	Scaling Factor	Sensitivity
Log (absolute permeability), m^2	−18.0	479	1.0	479
Van Genuchten parameter $1/\alpha$, MPa	1.0	1331	0.3	399
Van Genuchten parameter n	2.0	347	0.5	174
Vapor diffusion factor Ω^w	0.1	280	0.1	28
Porosity ϕ	0.01	2525	0.01	25
Van Genuchten parameter S_{lr}	0.0	247	0.1	25
Van Genuchten parameter η	0.5	188	0.1	19
Tortuosity τ	1.0	15	0.5	8
Van Genuchten parameter γ	0.333	36	0.1	4

number of parameters should be as small as possible, and the system response at the calibration points has to be sensitive to the unknown parameters. Furthermore, low correlation coefficients are desirable so that each parameter can be determined independently. In order to obtain this information, we define sensitivity coefficients for each parameter p_i as follows:

$$S_{pi} = \sum_{k=1}^{m} \left| \frac{\partial r_k}{\partial p_i} \right| (c_k)^{1/2} \tag{25}$$

where c_k is the kth diagonal element of the assembled covariance matrix **C**. In order to rank the parameters according to their impact on the objective function, the sensitivity measure (25) has to be scaled to account for the different units and potential ranges of each of the parameters. The sensitivity coefficients, scaling factors, and resulting sensitivities are summarized in Table 1. Even though the choice of the scaling factors is somewhat subjective, the analysis clearly indicates that log (k), $1/\alpha$, and n are the three most sensitive parameters. Furthermore, the covariance matrix (18) reveals that, for example, the two parameters n and S_{lr} are highly correlated and cannot be determined independently from water potential measurements alone. We therefore fix the less sensitive parameter S_{lr} at the value given in Table 1 and estimate only the van Genuchten parameter n. Consequently, the result of the optimization process has to be interpreted by considering the correlations between the estimated parameters and the fixed parameters, the latter being part of the conceptual model. We finally mention that this analysis reflects the sensitivities only at one point in the parameter space. Since the model is nonlinear, the sensitivity coefficients S_{pi} change if evaluated for different parameter combinations. Hence the analysis has to be repeated after completion of the optimization process. While the sensitivity coefficients changed, the ranking was found to be consistent with the one for the initial parameter set.

The analysis suggests estimation of three parameters, namely, the absolute permeability k and the parameters n and $1/\alpha$ of van Genuchten's characteristic curves described by (7) and (9). The initial guess for the absolute permeability of Grimsel granodiorite is taken from *Kull et al.* [1993] to be 10^{-18} m^2, and the empirical correlation observed by *Wang* [1992] is applied to obtain the initial guesses for the van Genuchten parameter n and $1/\alpha$. We employ a reparametrization for absolute permeability and estimate its logarithm instead of the value itself. A starting value is assigned to each of the unknown parameters, and the ITOUGH2 code is run, applying least squares optimization. Figure 4 shows observed data [*Gimmi et al.*, 1992] and computed water potentials at different depths from the drift surface and for a ventilation period of 80 days. The actual field data are represented by solid squares.

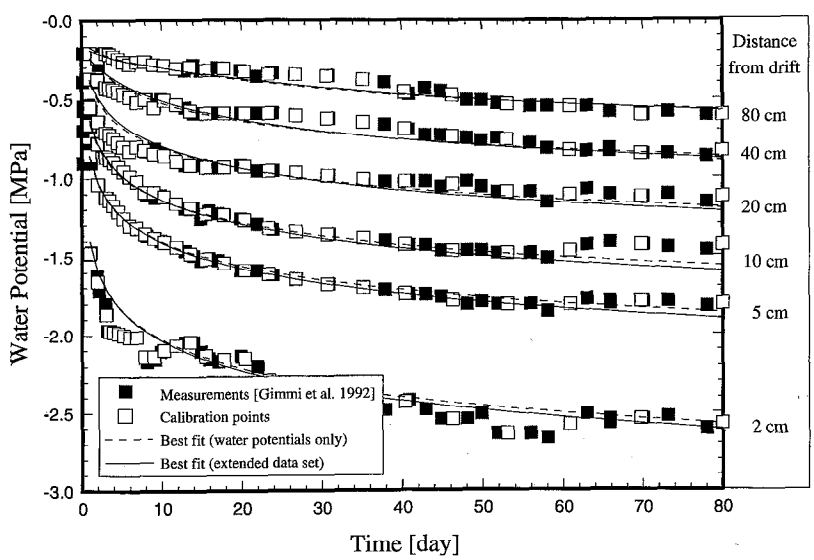

Figure 4. Fit between computed and measured water potentials. Data from *Gimmi et al.* [1992].

Table 2. Covariance (Diagonal and Lower Triangle) and Correlation (Upper Triangle) Matrices

	log (k)	n	$1/\alpha$
log (k)	6.49×10^{-3}	−0.72	−0.97
n	-2.34×10^{-3}	1.60×10^{-3}	0.64
$1/\alpha$	-3.91×10^{-3}	1.29×10^{-3}	2.49×10^{-3}

The calibration points, which are linearly interpolated between the data, are shown as open squares. The calculated solution is depicted as a dashed line. An alternative solution based on an extended data set is also shown (solid lines) and will be discussed later in the paper.

First, we note that the model is capable of reproducing the overall behavior of the two-phase flow system. Both the magnitude and the trend of the water potentials are well reproduced by the model results. This visual finding is confirmed by the estimated residual variance, $s_0^2 = 1.07$. Since the ratio $s_0^2/\sigma_0^2 = 1.07$ is smaller than the quantile $F_{153,\infty,95\%} = 1.24$, we conclude that the achieved match is consistent with our expectations regarding the final residuals. The calculated total inflow to the drift, however, is about three times higher than the one observed in the field. The results of the inversion are summarized in Table 2 (covariance and correlation matrices) and Table 3 (estimated parameter set, eigenvalues, and eigenvectors of the covariance matrix).

The correlation matrix reveals strong interdependencies between all parameters. Since decreasing the value for n reduces the liquid relative permeability, the absolute permeability has to be increased in order to maintain a certain water flow rate. This explains why n and log (k) are negatively correlated. Similarly, the water potentials decrease with higher air entry pressure and higher permeability, leading to a negative correlation between these two parameters. The correlation between n and $1/\alpha$ is difficult to predict because the effect of these parameters on capillarity changes with saturation. Since the propagation of the unsaturated front depends on absolute permeability, thus determining the saturation at each of the tensiometers, the correlation between the two van Genuchten parameters is indirectly affected by their correlation with log (k). The parameter combinations along the eigenvector with the largest eigenvalue are relatively unreliable.

From the discussion above it can be concluded that determining the absolute permeability by means of independent data may greatly reduce the correlations among all three parameters and therefore improve the quality of the estimation. In order to do this, we select the total inflow rate of moisture to the drift as an additional data point, expecting it to be a very sensitive measure with respect to changes in the absolute permeability. However, inflow measurements from larger drift sections contain significant contributions from highly conductive shear zones, which would lead to systematic errors. By covering these shear zones with plastic sheeting, the mean flow rate of water extracted from the granodiorite matrix is determined to be in the order of 0.3 mg s^{-1} m^{-2} [*Kull et al.*, 1991]. This is consistent with small scale measurements of evaporation rates at the drift wall, where values between 0.4 and 1.3 mg s^{-1} m^{-2} were observed during a short-term ventilation experiment with a relative humidity of 65% [*Vomvoris and Frieg*, 1991]. These values are somewhat higher than the average rate because they are taken at the beginning of a climatic change, when increased inflow is expected (see Figure 2).

We extend our set of calibration points by calculating the total inflow to the drift and compare it with the measured value given by *Kull et al.* [1991]. Furthermore, we include two gas pressure measurements in our model, taken in boreholes BOVE 84.011 and BOVE 84.018 (see Figure 1). The extent of the reduced pressure zone as shown in Figure 3 is reflected in these data. Pressures of 0.12 MPa and 0.28 MPa are observed in the relevant borehole intervals, respectively [*Vomvoris and Frieg*, 1991]. They are compared with the computed pressure at the end of the modeled ventilation period. Finally, we take the estimates of the previous run as prior information about the parameters.

The stochastic model for the extended data set is summarized in Table 4. Prior information is weighted by the inverse of the scaling factors shown in Table 1, and $(\sigma_0^2)_{pi}$ is set to 0.4, which slightly increases the importance of the penalty criterion. The standard deviation of the inflow measurement is assumed to be 0.05 mg s^{-1} m^{-2}. A value of 0.04 is chosen for the factor $(\sigma_0^2)_f$, accounting for the fact that the flow rate is a mean value which has to be appropriately weighted against the 150 individual water potential measurements. A standard deviation of 0.02 MPa is assigned to the residuals from the pressure measurements, and $(\sigma_0^2)_p$ is reduced by a factor of 4 with respect to the water potential measurements which serve as the reference data points with $(\sigma_0^2)_{wp} = 1$.

Next, the model is automatically calibrated by means of the Levenberg-Marquardt minimization algorithm. The Levenberg parameter μ in (14) is initialized to be 0.01 and is reduced by a factor of 10 after each successful iteration or increased accordingly if (13) results in an uphill step. Minimization is started from five different initial parameter sets to ensure that the procedure converges to a unique solution. The five initial parameter sets, the best estimates, and the final value of the objective function are summarized in Table 5. The reduction of the objective function along the solution path during the first five iterations is visualized in Figure 5a. The updated parameter values after each step are depicted in Figures 5b–5d for the parameters. Optimization is stopped if the scaled step length is smaller than a predefined value or if 10 consecutively unsuccessful steps were taken. This occurred after between four and seven iterations, requiring between 31 and 58 solutions of the direct problem. All five inverse runs resulted in parameter sets that are almost identical. From this finding we conclude that the solution is unique within a parameter space bounded by rather extreme, albeit physically reasonable, values, i.e., $-21.0 < \log(k) < -17.0$, $2.0 < n < 5.0$, and 0.5 MPa $< 1/\alpha <$ 2.5 MPa.

Inverse modeling results with the extended data set are summarized in Tables 6 and 7. First we note that appending flow rate and gas pressure data to the water potential measurements results in a slightly lower value for the absolute permeability. The other two parameters are shifted according

Table 3. Parameter Estimates, Eigenvalues, and Eigenvectors of Estimation Covariance Matrix

			Eigenvectors		
Parameter	Estimate	Eigenvalue	First	Second	Third
log (k), m^2	−18.29	9.75×10^{-3}	0.813	0.171	0.557
n	2.37	7.53×10^{-4}	−0.311	0.936	0.166
$1/\alpha$, MPa	1.59	7.75×10^{-5}	−0.493	−0.308	0.814

Table 4. Stochastic Model, Extended Data Set

Observation Type	Index j	Number of Data Points	$(\sigma_0^2)_j$	Diagonal Elements of Matrix $\mathbf{V}_j$
Prior information	pi	3	0.40	(scaling factors in Table 1)^2
Water potentials	wp	150	1.00	(0.1 × measured value)^2, MPa^2
Mean inflow	f	1	0.04	2.5×10^{-3} mg^2 s^{-2} m^{-4}
Gas pressure	p	2	0.25	4.0×10^{-4} MPa^2

to the correlation rules discussed above. This indicates that the solution of the inversion depends not only on the value of the observed state variable but also on the relative weighting between data of different types. Comparing Table 2 and Table 6 shows that the quality of the estimates has improved. This is mainly due to the fact that adding flow rate data allows a more independent determination of the absolute permeability, which results in a reduction in the correlation coefficients. Furthermore, weakening the indirect correlation between the two parameters n and $1/\alpha$ reveals that they are actually negatively correlated. Increasing either n or $1/\alpha$ affects the overall system behavior in the same direction, i.e., decreases water potentials (especially at the deep sensors) and enhances the inflow to the drift.

The calculated flow rate of 0.31 mg m^{-2} s^{-1} compares very well with the observed value of 0.3 mg m^{-2} s^{-1}. The difference between measured and calculated gas pressures is less than 0.01 MPa (see Figure 3). The predicted water potentials, plotted as solid lines in Figure 4, are very close to the measured values and the results from the previous calculation (dashed lines). This can be expected because the parameter set has been shifted basically along the eigenvector associated with the largest eigenvalue.

The relative permeability and capillary pressure function for the Grimsel granodiorite, as determined by inverting the data from the ventilation experiment, are shown in Figures 6 and 7, respectively. The impact of the parameter uncertainty on the shape of the characteristic curves is also visualized. The standard deviations are calculated by assuming linear error propagation, taking into account the correlation between n and $1/\alpha$. The parameters S_{lr}, η, and γ of van Genuchten's functions are assumed to be known exactly. The narrow error band is a result of both the good match that was achieved, resulting in a low estimated error variance s_0^2, and the high sensitivity of the observed system response with respect to the parameters n and $1/\alpha$.

In the remainder of this paper we demonstrate that the actual confidence region around the optimum parameter set can be accurately represented by a covariance matrix that is corrected to account for nonlinearities. For illustrative purposes we consider only two parameters, n and $1/\alpha$. The two-dimensional ellipse shown below thus represents the conditional confidence region of the three-dimensional ellipsoid (Table 6), assuming that the absolute permeability is known exactly. By evaluating the objective function for many parameter combinations, a contour map can be drawn (Figure 8), depicting the location and convexity of the minimum.

Table 5. Best Estimates Obtained Starting From Five Different Initial Parameter Sets

Set	Parameter	Initial Guess	Iterations/ Direct Runs	Final Objective Function	Best Estimate
1	log (k), m^2	−17.00	6/39	159.3	−18.58
	n	3.00			2.48
	$1/\alpha$, MPa	0.50			1.74
2	log (k), m^2	−18.00	7/58	159.2	−18.56
	n	2.00			2.47
	$1/\alpha$, MPa	1.00			1.74
3	log (k), m^2	−19.00	5/35	160.2	−18.58
	n	2.50			2.47
	$1/\alpha$, MPa	2.00			1.75
4	log (k), m^2	−20.00	6/45	159.0	−18.58
	n	5.00			2.48
	$1/\alpha$, MPa	1.50			1.74
5	log (k), m^2	−21.00	4/31	159.2	−18.56
	n	4.00			2.48
	$1/\alpha$, MPa	2.50			1.73

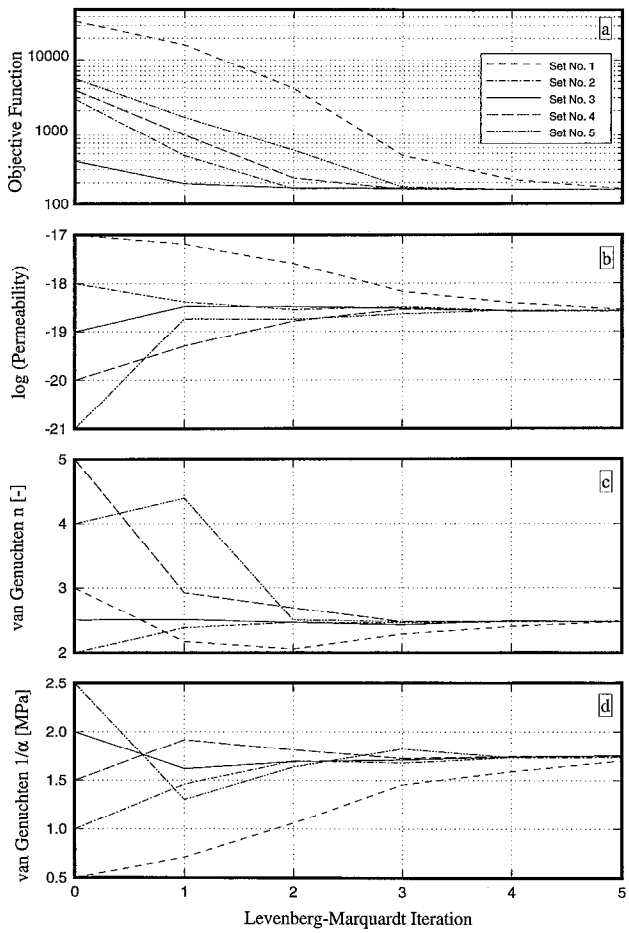

Figure 5. Performance of Levenberg-Marquardt algorithm during minimization. (a) Reduction of objective function; (b) update of parameter log (k); (c) update of parameter n; (d) update of parameter $1/\alpha$.

Table 6. Covariance (Diagonal and Lower Triangle) and Correlation (Upper Triangle) Matrices, Extended Data Set

	log (k)	n	$1/\alpha$
log (k)	3.84×10^{-4}	−0.27	−0.58
n	-1.59×10^{-4}	9.14×10^{-4}	−0.32
$1/\alpha$	-2.01×10^{-4}	1.71×10^{-4}	3.12×10^{-4}

From (15) we see that the actual confidence region on a given significance level α is bounded by the contour of the objective function on level $\zeta(\hat{\mathbf{p}}) + s_0^2 n F_{n,m-n,1-\alpha}$. For two parameters and 155 data points, the quantile of the F distribution on the 95% confidence level is $F_{2,153,0.95} = 3.054$. The linear approximation of this confidence region is given by (20). We then increase the corresponding eigenvalues, following the procedure outlined in section 3.3. As a result, the actual confidence region is accurately represented by an ellipse, the orientation of which is calculated from the standard linear error analysis, and its size is appropriately corrected to account for nonlinearities. The increase in the eigenvalues which is necessary to better approximate the actual confidence region shows that linear error analysis provides too optimistic a measure of the estimation error. This is because (20) intrinsically describes a minimum variance bound. Furthermore, it is shown that the shape of the actual confidence region is close to ellipsoidal, so that its description by means of a covariance matrix seems justified in this case. Finally, the approximation of the Hessian by the matrix $\mathbf{J}^T\mathbf{V}^{-1}\mathbf{J}$ is accurate enough to derive the orientation of the confidence region, i.e., the eigenvectors of the covariance matrix (18). This concludes the discussion of the nonlinear error analysis.

5. Concluding Remarks

Three major aspects of inverse modeling in groundwater hydrology have been addressed in this paper.

1. The problem of parameter estimation is solved for the simulation of groundwater systems that contain two immiscible fluids. While the direct measurement of two-phase parameters is both conceptually difficult and experimentally expensive, inverse modeling provides an appealing technique to obtain model-related parameters by calibrating the numerical model against sensitive observations of the system state.

2. The inverse problem is formulated in the framework of maximum likelihood estimation theory. The objective function from generalized least squares optimization is minimized by using the Levenberg-Marquardt algorithm. The efficiency of the procedure allows examination of different model structures and different data sets, improving the understanding of the two-phase flow system. Furthermore, the analysis of sensitivity coefficients and the correlation structure provides some guidance for the design of future experiments.

3. One of the main advantages of inverse modeling is that the quality of the estimation can be described by statistical measures. However, if the model is highly nonlinear, the standard linear error analysis overestimates the accuracy of the optimum parameter set. Based on an idea originally presented by *Carrera* [1984], we calculate a corrected covariance matrix which approximates the true confidence region in the nonlinear case. The procedure is computationally inexpensive and leads to easily reportable confidence regions.

The method of parameter estimation by inverse modeling has been applied to data from a ventilation test performed at

Table 7. Parameter Estimates, Eigenvalues, and Eigenvectors of Estimation Covariance Matrix, Extended Data Set

			Eigenvectors		
Parameter	Estimate	Eigenvalue	First	Second	Third
log (k), m^2	−18.56	5.52×10^{-4}	0.758	−0.193	0.624
n	2.47	9.79×10^{-4}	0.024	0.963	0.268
$1/\alpha$, MPa	1.74	7.86×10^{-5}	−0.652	−0.188	0.734

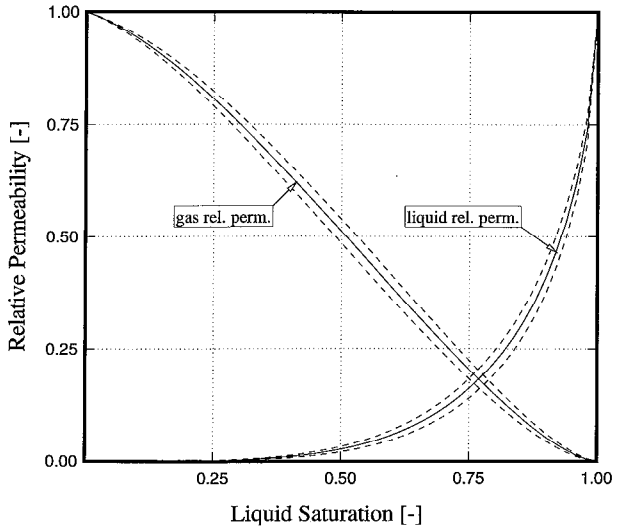

Figure 6. Gas and liquid relative permeabilities (rel. perm.) for Grimsel granodiorite. The parameters of van Genuchten's function are determined by inverse modeling; dashed lines indicate the 95% error band.

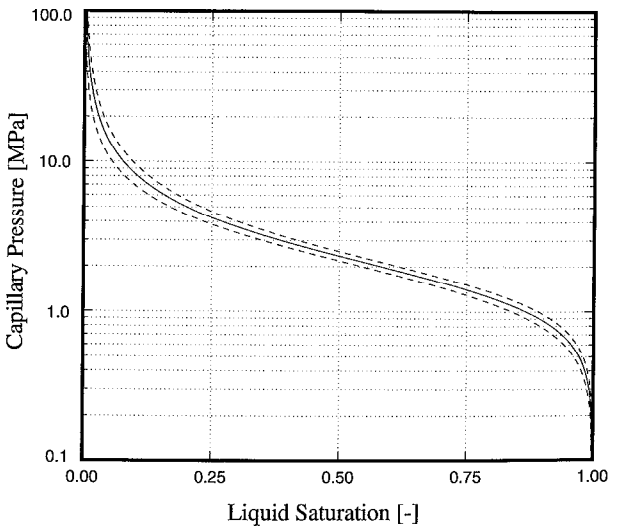

Figure 7. Capillary pressure function for Grimsel granodiorite. The parameters of van Genuchten's function are determined by inverse modeling; dashed lines indicate the 95% error band.

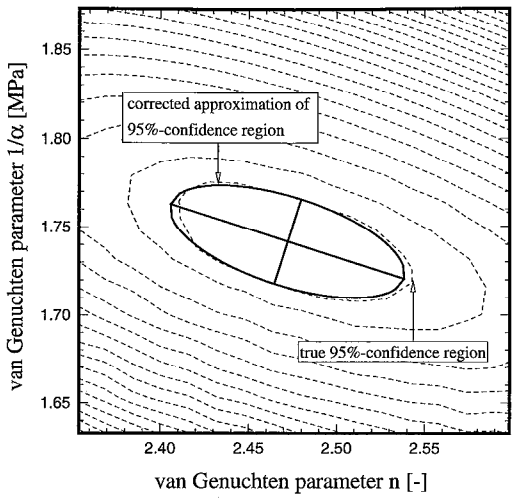

Figure 8. Contours of objective function, true confidence region, and corrected approximation of confidence region to account for nonlinearities.

the Grimsel Rock Laboratory. The following major conclusions can be drawn from this field application.

1. We successfully modeled a field experiment conducted under two-phase flow conditions. The conceptual model incorporates a variety of physical processes, including evaporation at the drift surface, capillary forces and phase interferences, and binary diffusion of water vapor and air, driven by vapor pressure-lowering effects. A sensitivity analysis has been performed to assess the main features of the conceptual model. Since the system response is sensitive to the input parameters of the numerical model, observations of different types can be used to determine the properties of interest.

2. Inverse modeling of the ventilation experiment provides reliable estimates of model-related formation parameters affecting two-phase flow. If the absolute permeability can be determined independently, the parameters of van Genuchten's characteristic curves are estimated with less uncertainty because of a more favorable correlation structure.

3. If the model is strongly nonlinear in the parameters, the standard way of calculating error bounds on the parameters leads to too optimistic variances. The nonlinear error analysis proposed in this paper provides an improved estimate of the confidence region.

Acknowledgments. This work was carried out under U.S. Department of Energy contract DE-AC03-76SF00098 for the Director, Office of Civilian Radioactive Waste Management, Office of External Relations, and was administered by the Nevada Operations Office, U.S. Department of Energy, in cooperation with the Swiss National Cooperative for the Disposal of Radioactive Waste (Nagra). Much of this paper is based on research performed at the Laboratory of Hydraulics, Hydrology and Glaciology (VAW), ETH Zürich, in collaboration with Nagra. We are especially grateful to J. Trösch and U. Kuhlmann (VAW) and S. Vomvoris (Nagra) for their support. We would also like to thank T. Gimmi, Institute of Terrestrial Ecology, ETH Zürich, for providing most of the input data of the field example. We thank C. Doughty, G. Moridis and J. Najita, Lawrence Berkeley Laboratory, and two anonymous reviewers for their helpful comments.

References

Carrera, J., Estimation of aquifer parameters under transient and steady state conditions, Ph.D. dissertation, Dep. of Hydrol. and Water Resour., Univ. of Ariz., Tucson, 1984.

Carrera, J., and S. P. Neuman, Estimation of aquifer parameters under transient and steady state conditions, 1, Maximum likelihood method incorporating prior information, *Water Resour. Res.*, *22*(2), 199–210, 1986.

Chavent, G., On the theory and practice of non-linear least-squares, *Adv. Water Resour.*, *14*(2), 55–63, 1991.

Connell, L. D., and P. R. F. Bell, Modeling moisture movement in revegetating waste heaps, 1, Development of a finite element model for liquid and vapor transport, *Water Resour. Res.*, *29*(5), 1435–1443, 1993.

Donaldson, J. R., and R. B. Schnabel, Computational experience with confidence regions and confidence intervals for nonlinear least squares, *Technometrics*, *29*(1), 67–82, 1987.

Edlefsen, N. E., and A. B. C. Anderson, Thermodynamics of soil moisture, *Hilgardia*, *15*(2), 31–298, 1943.

Finsterle, S., Inverse Modellierung zur Bestimmung hydrogeologischer Parameter eines Zweiphasensystems, Mitt. 121, Versuchsanst. für Wasserbau, Hydrol. und Glaziol., Eidg. Tech. Hochsch., Zürich, Switzerland, 1993a.

Finsterle, S., ITOUGH2 user's guide, *Rep. LBL-34581*, Lawrence Berkeley Lab., Berkeley, Calif., 1993b.

Gimmi, T., H. Wydler, T. Baer, H. Abplanalp, and H. Flühler, Near field desaturation experiment at the Grimsel Test Site (FLG), *Intern. Rep.*, Nagra, Wettingen, Switzerland, 1992.

International Formulation Committee, A formulation of thermodynamic properties of ordinary water substance, report, IFC Secretariat, Düsseldorf, Germany, 1967.

Kool, J. B., J. C. Parker, and M. T. van Genuchten, Parameter estimation for unsaturated flow and transport models—A review, *J. Hydrol.*, *91*, 255–293, 1987.

Kull, H., W. Brewitz, and K. Klarr, Felslabor Grimsel: Ventilationstest—In-situ-Verfahren zur Permeabilitätsbestimmung im Kristallin, *Tech. Rep. NTB 91-02*, Nagra, Wettingen, Switzerland, 1991.

Levenberg, K., A method for the solution of certain nonlinear problems in least squares, *Q. Appl. Math.*, *2*, 164–168, 1944.

Luckner, L., M. T. van Genuchten, and D. Nielsen, A consistent set of parametric models for the two-phase flow of immiscible fluids in the subsurface, *Water Resour. Res.*, *25*(10), 2187–2193, 1989.

Marquardt, D. W., An algorithm for least-squares estimation of nonlinear parameters, *J. Soc. Ind. Appl. Math.*, *11*(2), 431–441, 1963.

Mualem, Y., A new model for predicting the hydraulic conductivity for unsaturated porous media, *Water Resour. Res.*, *12*(3), 513–522, 1976.

Narasimhan, T. N., and P. A. Witherspoon, An integrated finite difference method for analyzing fluid flow in porous media, *Water Resour. Res.*, *12*(9), 57–64, 1976.

Neuman, S. P., Calibration of distributed parameter groundwater flow models viewed as a multiple-objective decision process under uncertainty, *Water Resour. Res.*, *9*(4), 1006–1021, 1973.

Peaceman, D. W., *Fundamentals of Numerical Reservoir Simulation*, Elsevier, New York, 1977.

Pruess, K., TOUGH user's guide, *Nucl. Regul. Comm. Rep. LBL-20700*, Lawrence Berkeley Lab., Berkeley, Calif., 1987.

Pruess, K., TOUGH2—A general-purpose numerical simulator for multiphase fluid and heat flow, *Rep. LBL-29400*, Lawrence Berkeley Lab., Berkeley, Calif., 1991.

Pruess, K., and T. N. Narasimhan, A practical method for modeling fluid and heat flow in fractured porous media, *Soc. Pet. Eng. J.*, *25*(1), 14–26, 1985.

Scales, L. E., *Introduction to Non-linear Optimization*, Springer-Verlag, New York, 1985.

Seager, M., A SLAP for the masses, *Tech. Rep. UCRL-100267*, Lawrence Livermore Natl. Lab., Livermore, Calif., 1988.

Sun, N.-Z., and W. W.-G. Yeh, Coupled inverse problems in groundwater modeling, 1, Sensitivity analysis and parameter identification, *Water Resour. Res.*, *26*(10), 2507–2525, 1990.

van Genuchten, M. T., A closed form equation for predicting the hydraulic conductivity of unsaturated soils, *Soil Sci. Soc. Am. J.*, *44*(5), 892–898, 1980.

Vargaftik, N. B., *Tables on the Thermophysical Properties of Liquids and Gases*, 2nd ed., John Wiley, New York, 1975.

Vomvoris, S., and B. Frieg (Eds.), Grimsel Test Site: Overview of Nagra field and modeling activities in the Ventilation Drift (1988–1990), *Tech. Rep. NTB 91-34*, Nagra, Wettingen, Switzerland, 1991.

Walker, W. R., J. D. Sabey, and D. R. Hampton, Studies of heat transfer and water migration in soils, Dep. of Agric. and Chem. Eng., Colo. State Univ., Fort Collins, 1981.

Wang, J. S. Y., Variations of hydrological parameters of tuff and soil, in *Proceedings of the Third International High Level Radioactive Waste Management Conference*, pp. 722–731, American Nuclear Society, La Grange Park, Ill., and American Society of Civil Engineers, New York, 1992.

Xiang, Y., S. F. Sykes, and N. R. Thomson, A composite L_1 parameter estimator for model fitting in groundwater flow and solute transport simulations, *Water Resour. Res.*, *29*(6), 1661–1673, 1993.

Yeh, W. W.-G., Review of parameter estimation procedures in groundwater hydrology: The inverse problem, *Water Resour. Res.*, *22*(2), 95–108, 1986.

S. Finsterle and K. Pruess, Earth Sciences Division, Lawrence Berkeley Laboratory, University of California, Berkeley, CA 94720.

(Received December 8, 1993; revised November 11, 1994; accepted November 17, 1994.)